**Carbon Cathode Wear in Aluminium Electrolysis Cells**

Samuel Senanu[1,2], Zhaohui Wang[1,2], Arne Petter Ratvik[2*] and Tor Grande[1]
1. Department of Material Science and Engineering, NTNU Norwegian University of Science and Technology, NO-7491 Trondheim, Norway
2. SINTEF Industry, NO-7465 Trondheim, Norway
*Corresponding author: arne.p.ratvik@sintef.no

Keywords: Cathode wear, graphitic cathode, pitting, current density, particle detachment.

## Abstract

Autopsies of six spent potlinings with different carbon cathode block grades, amperage regimes and cell design were conducted at three separate smelters to reveal possible mechanisms causing cathode wear. Microstructure of the cathode samples from the autopsies was investigated by optical and electron microscopy and X-ray computed tomography, while the composition of solid bath at the surface and in the interior pores were investigated by X-ray diffraction and electron microscopy. The present findings revealed that the cathode surface was characterized by a wear pattern resembling pitting corrosion, and it is discussed that the observed variations in the bath chemistry plays a major role for the wear mechanism and the pitting of the surface. A hypothesis involving initiation and termination of the main reaction causing the cathode wear is proposed based on the effect of the consumption of aluminium fluoride in the molten bath layer between the carbon and the molten aluminium pad, resulting in partly solidification of the bath and spatial variation of the current density.

## Introduction

Carbon cathode wear in the aluminium industry has been a very important topic in the last few decades, particularly due to the change to high amperage regimes coupled with the use of highly graphitized cathode blocks and more acidic baths [1]. Even though the industry has benefited in terms of increased productivity, lower energy consumption and reduced sodium expansion [2, 3], the cathode life has become a critical issue , resulting in higher costs due to relining of new cells and disposal of the spent potlinings [3].

Autopsies of spent potlinings have shown a so-called W or WW wear pattern, while locally the wear is characterized by pitting, especially at locations with the highest wear [1, 4-7]. The W or WW wear pattern is suggested to result from the variation of the current density across the carbon blocks [5, 8, 9]. The more pronounced wear in case of the more graphitized cathode blocks can be related to the electrical conductivity and uneven distribution of the current density [9]. It has also been reported that the more graphitized cathode blocks wear faster than less graphitized cathode blocks [4], while laboratory experiments have not been conclusive on this [3, 10].

Infiltration of sodium and electrolyte in the carbon cathodes are important factors for understanding cathode wear [1, 10-11]. Moreover, cathode wear is also closely related to the formation of $Al_4C_3$ by the reaction [11]

$$4\ Na_3AlF_6(l) + 12\ Na\ (in\ C) + 3\ C = Al_4C_3 + 24\ NaF(l) \quad (1)$$

Formation of $Al_4C_3$ inside the pores in the carbon cathodes was reported by Lossius and Øye [12]. Formation of $Al_4C_3$ within the porous carbon binder pitch may lead to degradation and enhanced wear by a particulate detachment mechanism as discussed by Rafiei et al. [1], Patel et al. [11] and Siew et al. [13]. However, a recent characterization of pitting did not correlate with the aggregate size in the cathode, not supporting particulate detachment as the main wear mechanism [14].

Autopsies of spent potlinings are an important method used to understand catastrophic and normal cathode failures, diagnose integrity of linings (for new cell designs) prior to load increase, monitor post mortem cell performance, and to study the mineralogy and chemistry of the linings. Autopsies of spent potlinings may also contribute to identify mechanism(s) leading to carbon cathode wear [3, 15-19]. The autopsy technique involves different procedures such as visual observations and measurement of the wear patterns and analysing autopsy samples using electron and optical microscopy as well as X-ray computed tomography. Tools like cameras and 3D laser scanners are currently used to obtain detailed information of the wear patterns [20].

The present paper reports on autopsy findings from six different spent potlinings with different grades of carbon cathode blocks (graphitic and graphitized) at three smelters with different amperage regimes and cell designs.

Parts of the results from the autopsies have been reported in previous reports [7, 14]. The macroscopic wear pattern was characterized by interferometry, while the microstructure and topography close to the upper surface of the samples collected from the autopsies were characterized by X-ray computed tomography, X-ray diffraction and microscopy. A mechanism for uneven local wear is proposed based on partly solidification of the bath film at the carbon surface due to the formation of aluminium carbide. Finally, Finite Element Model (FEM) simulation was used to confirm the spatial distribution of the current at the cathode surface due to partly solidification of the bath caused by the formation of aluminium carbide.

## Experimental

Autopsy and sampling

A summary of the six pots investigated is given in Table 1. After the pots were shut down they were allowed to cool over a couple of days in a dry and an enclosed area. Metal and bath were then carefully removed from the top surface of the carbon cathode before the cathode surface was vacuum cleaned.

**Table 1** Summary of wear patterns and details of the pots investigated during the autopsy studies

| Pot | Arrangement/ Technology | Amperage(kA)/ Cathode Current density (A/cm$^2$) | Pot age (days) | Carbon Cathode Block type | Wear Pattern | Comments |
|---|---|---|---|---|---|---|
| 1 | Side by Side / Prebaked | 313 / 0.8 | 2461 | Graphitized and Impregnated | WW | Planned Shutdown |
| 2 | End to End / Prebaked | 175 / 0.8 | 1028 | Graphitic (100 % Graphite) | W | Tapout |
| 3 | End to End / Prebaked | 175 / 0.8 | 3154 | Graphitic (100 % Graphite) | W | Planned Shutdown |
| 4 | End to End / Prebaked | 175 / 0.8 | 2849 | Graphitic (100 % Graphite) | W | Planned Shutdown |
| 5 | Side by Side / Prebaked | 313 / 0.8 | 1731 | Graphitized and High Density | WW | Tapout |
| 6 | Søderberg | 128 / 0.6 | 2732 | Amorphic (30 % Graphite) | Even | Planned Shutdown |

The topography of the spent potlinings was determined by optical photography and laser interferometry. Details such as pitting, potholes, sludge, cracks, metal plugs, etc. were captured using a camera, whilst the wear patterns or wear profiles were measured using a 3D Freestyle scanner. Data from the 3D scanning was also used to characterize the pitting observed on the carbon cathodes using the MeshLab software. Manual measurements and characterizations were also performed in some cases to document the wear pattern or profile across the cathode surface. Samples of solidified bath were collected from the bath on top of the metal pad and on the surface where the wear was highest. Cylindrical carbon samples were drilled out using an electrical drilling machine. A representative autopsy sample in a region with considerable wear and pitting is shown in Figure 1.

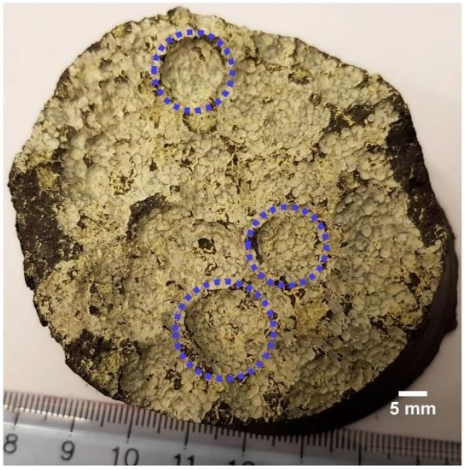


**Figure 1** Cylindrical sample drilled from the spent potlining for laboratory analysis (CT and microscopy), showing pitting at the surface marked by the blue dotted circle

Characterization of samples from the autopsies

Carbon cathode and solid bath samples, collected during the autopsies, were analysed using different laboratory techniques such as X-ray computed tomography (CT scanning), X-ray diffraction (XRD), optical and scanning electron microscopy. CT scanning and optical microscopy were employed to characterize the microstructure, whilst X-ray diffraction and scanning electron microscopy, combined with Energy Dispersive Spectroscopy (EDS), were used to determine compositions of the solid bath on the cathode surface as well as in the pores. X-ray computed tomography was conducted using a Nikon XTH225ST instrument (cone beam volume CT), and details of the operation is given elsewhere [7]. Optical microscopy was performed using the REICHERT MeF3A optical microscope, whilst a Hitachi S-3400N was used for the scanning electron microscopy. XRD was performed using the D8 Advance X-ray diffractometer. The samples investigated were crushed, milled and sieved to obtain powder with the appropriate fine grain size. The samples analysed included the thin layer of bath in contact with the carbon cathode, frozen bath from the bath on top of metal pad, and samples further down into the cathode. Prior to microscopy, the samples were cut into smaller samples, which were imbedded into epoxy or current conducting polyfax and mechanically polished to obtain smooth surfaces.

FEM simulations

FEM simulation (2D, stationary) of a simplified thin film on a carbon cathode surface was conducted to support the hypothesis presented in this study. The simulations were performed using the COMSOL Multiphysics 5.3 program. The model consisted of a thin bath film on carbon cathode surface. By applying a potential across the thin bath film in a vertical direction, the current density along the carbon cathode at the locations with either liquid or solid bath was modelled. The electrical conductivities of the liquid and solid bath were set to 214 and 2.14 S/m, respectively, while that of the carbon cathode was set to $10^5$ S/m. Thickness of the bath film was 50 µm, while the potential applied across this film was chosen to be 3 mV. Assumptions made included that the thin bath film was mainly cryolite with no droplets of Al, implying only ionic conductivity in the bath layer as well as mainly vertical direction of the current. The governing equation for this model is $V = IR$ , where V is the voltage drop across the bath film in volts, I is the current in amperage and R is the electrical resistance within the bath film in ohm.

## Results

The autopsies of five of the pot linings revealed trends in the microscopic wear patterns similar to previously reported autopsy findings [4, 5, 7, 20]. The highest wear was observed on the carbon cathode blocks directly under the anode positions closer to the side ends of the cathode blocks, while the least wear was observed under the centre channel. Pot 6, which was a Søderberg pot, showed a relatively even wear across the whole cathode block. The observed wear patterns are summarized in Table 1. In the prebaked cathodes the wear was less severe in the ramming joints relative to the cathode blocks. Pitting of the surface of the carbon cathodes were observed for all the six spent potlinings, see Figure 1. For the prebaked pots the pitting was very distinct at the locations with the highest wear such as close to the side ends of the potlinings [4, 7]. A 3D image of a section of the potlining from pot 5 is shown in Figure 2a. The image demonstrates the high degree of pitting at the side ends of the spent potlining. Figure 2b shows the variation in size of the pitting from the centre channel to the side end of spent potline 3.

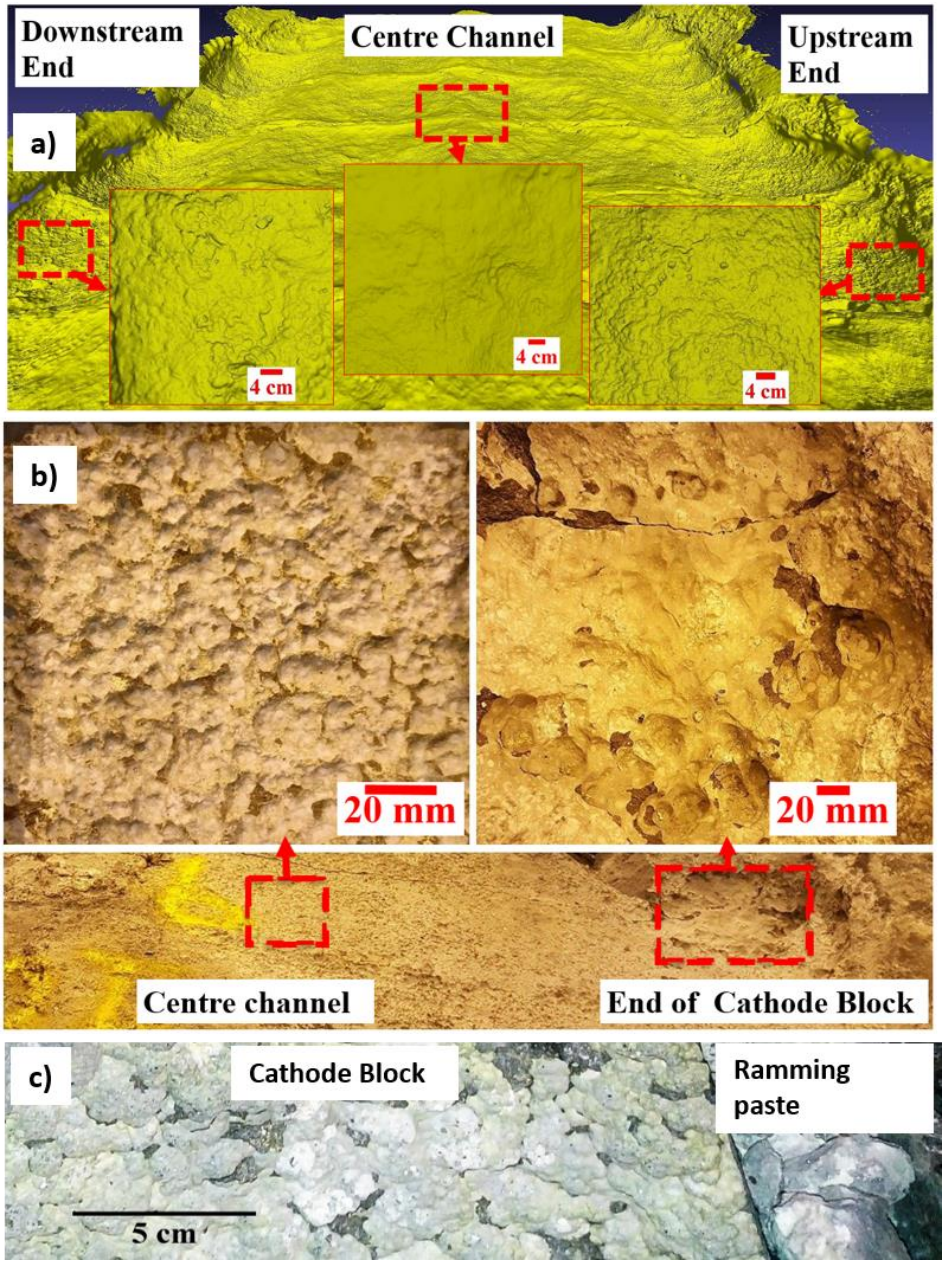


**Figure 2** Images of pitting on the surface of the carbon cathodes. **a** 3D scanning image of a section of pot 5 showing pitting at the ends of the cathode blocks**, b** Variation of pitting size along cathode block from side end to centre channel of the cell from pot 3, the typical pitting are highlighted with a red dashed rectangles**, c** Pitting on both cathode block and ramming joint from pot 5

A typical picture of the pitting observed at the locations with highest wear is shown in Figure 2c. It was observed that the pitting occurred on both the cathode block and ramming joint. Closer observations of the locations around the potholes, which developed to tapouts for pots 2 and 5, showed high levels of pitting. Finally, a thin layer of solidified bath was observed over the entire cathode surface in all the 6 spent potlinings.

A typical example of a CT scanning image demonstrating the topography of the cathode surface is shown in Figure 3. The light regions in the image correspond to solidified electrolyte in the open pores in the cathode, while the different shades of grey regions correspond to carbon. The border towards the black areas gives a detailed image of the worn surface. It was observed from the CT images that the carbon cathodes, including both the cathode block and ramming joints, were fully impregnated by bath. The ramming joints contained a larger amount of bath than the carbon cathode blocks owing to their higher porosity. The CT images demonstrate clearly an uniformly worn out surface over the binder matrix and aggregates within the cathode block. No observation of particulate detachment could be identified by CT scanning images.

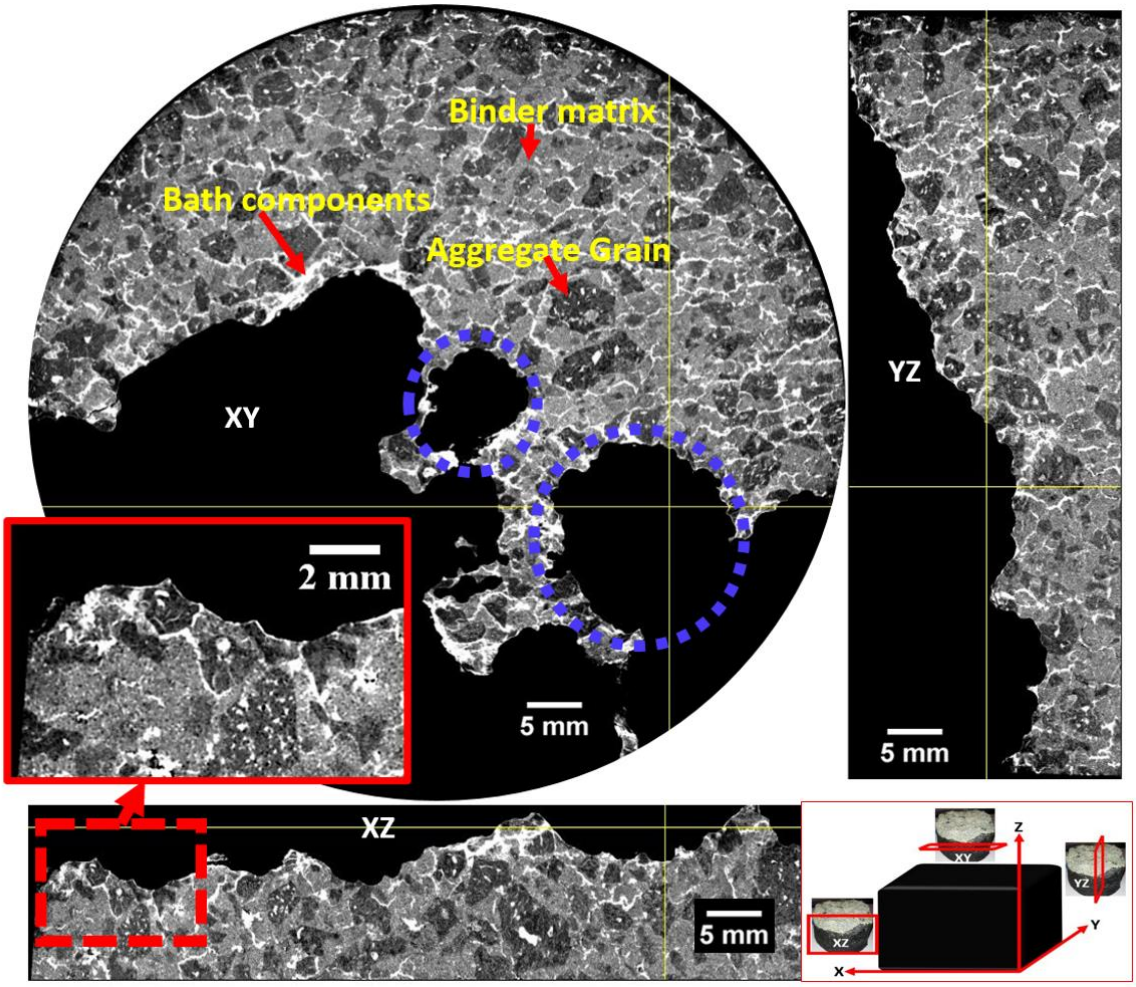


**Figure 3** CT scanning images of the XY, YZ and XZ directions with a highlighted section of the XZ directional view image to illustrate wear profile of binder matrix and aggregate. Pitting locations are marked by blue dotted circle on the XY image. A sketch defining the XY, YZ and XZ directions of the cylindrical cathode sample where the XY plane is normal to the Z-axis is included in the figure.

A typical optical micrograph of the carbon-bath interface is shown in Figure 4. The microstructure close to the surface of the cathode was qualitatively similar for all the samples. Closer examination of the optical micrographs exposed the wear profile along the interface with respect to the carbon components (binder matrix and aggregate). Both the aggregate and binder matrix components wear evenly with no discontinuity between aggregates and binder matrix. A thin layer of what was assumed to be aluminium carbide was observed in direct contact with the carbon cathode at the outer surface towards the bath. Other phases interpreted to be aluminium oxide and droplets of aluminium were also observed.

EDS element mapping of the carbon-bath interface, shown in Figure 5, revealed that the phase in direct contact with the carbon cathode was aluminium carbide in hydrated or non-hydrated form. It also showed the presence of cryolite bath, alumina and droplets of aluminium at the interface, and these phases were always observed to be above the aluminium carbide layer. In the Søderberg case, typically alumina sludge was observed on top of the aluminium carbide layer as shown in Figure 5a. In some cases the solidified electrolyte was observed above the aluminium carbide layer as shown in Figure 5b. The latter correspond to the situation observed in all the other prebaked pots.

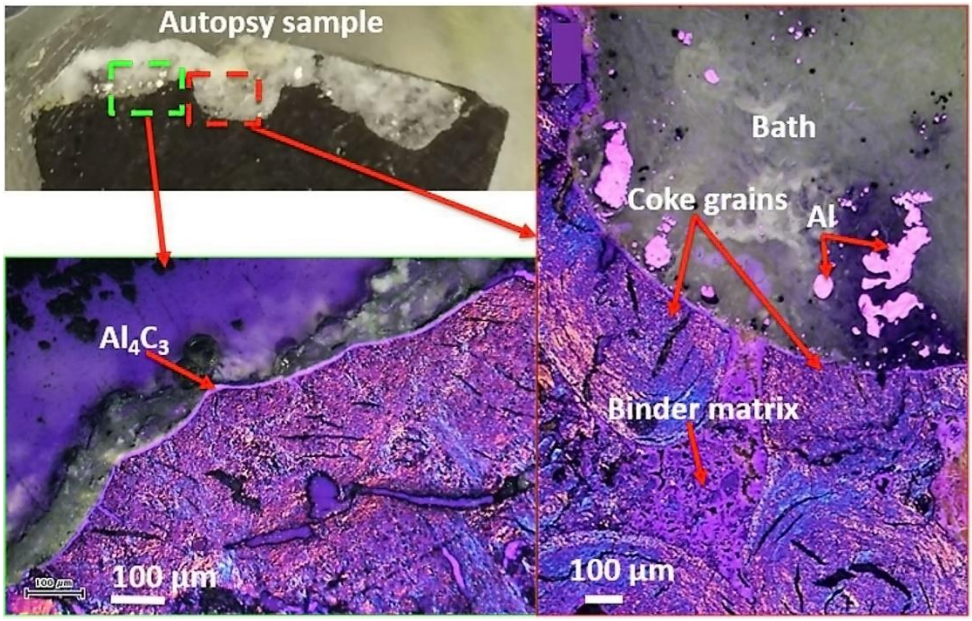


**Figure 4** Optical micrograph of the interface between the carbon cathode and bath in a sample from pot 1

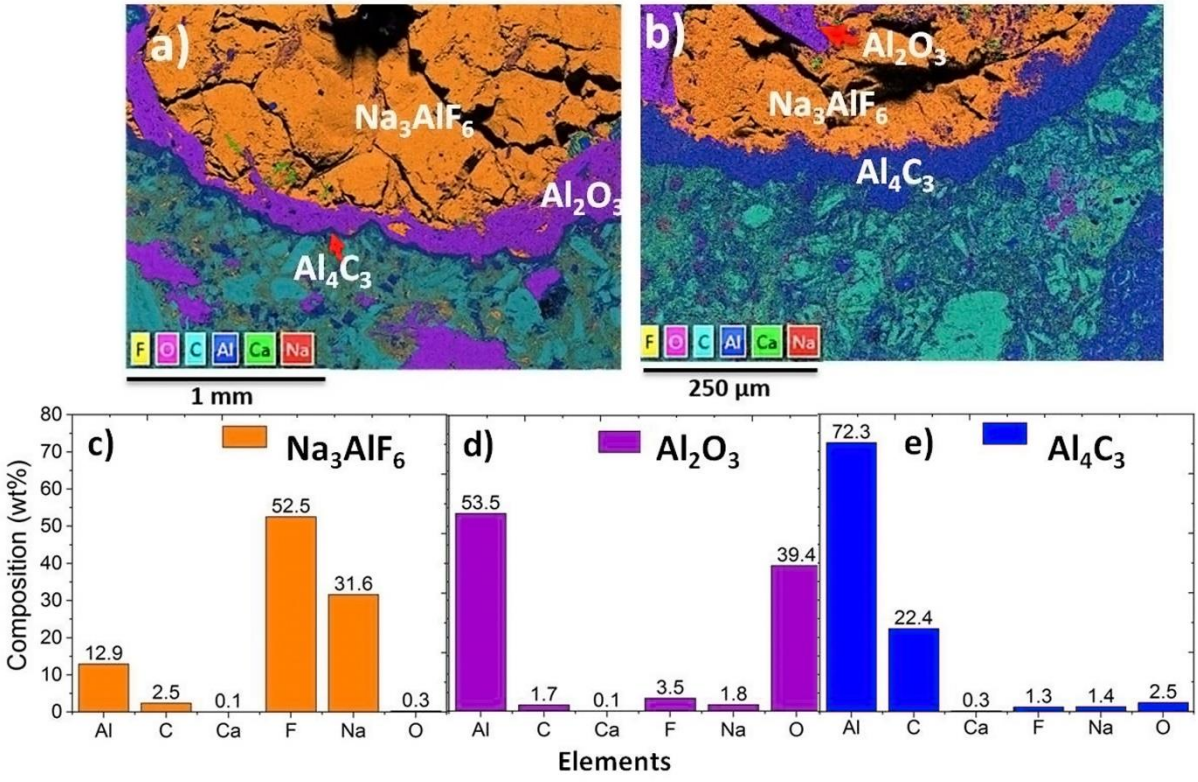


**Figure 5** EDS element mapping of carbon-bath interface of samples from pot 6. **a** Element map of cathode surface with sludge (pot 6), **b** Element map of cathode surface with no sludge, **c** Chemical composition of cryolite at interface, **d** Chemical composition of alumina at interface **e** Chemical composition of aluminium carbide at interface.

X-ray diffraction patterns of the solidified bath collected from the cathode surface (cathode surface bath) and electrolyte above the metal pad (main bath) are shown in Figure 6. The solid bath collected from the electrolyte above the metal pad contained the expected phases reflecting the compositions of a standard industrial electrolyte. The phase composition of the solid bath close to the cathode surface was significantly different consisting mainly

of $CaF_2$ and $Na_3AlF_6$ in addition to minor amounts of $Al_2O_3$ (not shown in the diffractogram). The phases observed for the cathode surface bath suggest a more basic bath as compared to the main bath. This supports a hypothesis that a chemical or electrochemical reaction, taking place at the cathode surface, results in depletion of $AlF_3$ in the electrolyte at the cathode surface in line with reaction 1 [21].

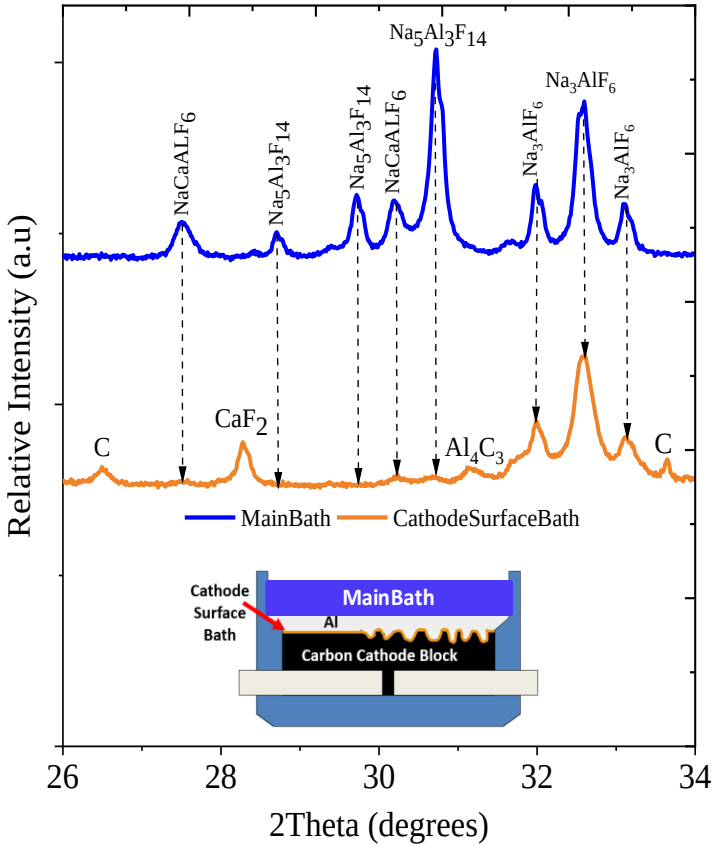


**Figure 6** X-ray diffraction pattern of bath samples collected from the bath on top of the metal pad and on top of the cathode surface. Black dashed arrows to trace the identified phases. Insert: sketch of an electrolysis cell showing locations of the solid bath samples

## Discussion

Pitting was observed on both the carbon cathode blocks and the ramming joints for all the spent potlinings studied. The characteristic pitting was more pronounced at locations such as the side ends as demonstrated in Figure 2a. The CT images (Figure 3) give a detailed view of the microstructure and the wear of the binder matrix and aggregate in the cathode materials. The uniformly worn aggregate grains within the carbon matrix suggest a chemical or electrochemical corrosion process involving aluminium carbide formation, dissolution and transport [3]. Hence, carbide formation within the matric, weakening of the carbon / grain-to-grain attachment and particulate detachment would be less likely to occur [1]. Optical micrographs of the carbon-bath interface, as shown in Figure 4, confirmed the CT findings that remains of uniformly worn out binder and aggregate components were present within the carbon matrix. Evidence for particulate detachment could not be found and the relatively uniform wear of the aggregate grains shown by both CT and optical microscope images suggest a chemical or electrochemical etching process. Optical micrographs and EDS element mapping, as shown in Figures 4 and 5, demonstrate the presence of aluminium carbide, cryolite, alumina and droplets of aluminium at the interface. Apart from the Søderberg pot samples that was dominated by alumina (sludge) on top of the aluminium carbide layer, the general trend was solidified bath above the aluminium carbide layer as shown in Figures 5a and 5b. Alumina on top of the carbon cathode is proposed to retard the wear reaction since alumina does not react with carbon. In addition, alumina limits the access of bath to the carbon surface for both carbide formation and carbide dissolution.

X-ray diffraction of solid bath samples collected from the main bath and the cathode surface (Figure 6) revealed that the composition at the carbon cathode surface differs from that of the electrolyte on top of the metal pad. The phases found in the bath at the cathode surface consisted mainly of $CaF_2$, $Na_3AlF_6$ and $Al_2O_3$ corresponding to a neutral or basic bath. The ternary phase diagram $Na_3AlF_6$ -$AlF_3$ -$CaF_2$ provided by Craig and Brown [22], shows that the typical solidified electrolyte corresponds to the solid phases $NaCaAlF_6$, $Na_5Al_3F_{14}$ and $Na_3AlF_6$. The phases found in the solid electrolyte close to the cathode surface show that the bath is depleted on $AlF_3$. Consumption of $AlF_3$ moves the bath composition towards the binary alkemade line $CaF_2$ - $Na_3AlF_6$ in the ternary diagram, where only $CaF_2$ and $Na_3AlF_6$ are present. This is consistent with the findings from X-ray diffraction (Figure 6) (the depletion of $AlF_3$ is proposed to be due to chemical or electrochemical reactions occurring at the cathode surface, in line with Reaction 1 [21]). The cooling of the spent pot lining may contribute to segragation of fluoride phases in the electrolyte, which should be followed up in future investigations of wear.

The shift to a relatively basic bath at the cathode surface also points to the importance of continuous supply of fresh bath to the cathode surface for cathode wear. Laboratory tests by Wilkening and Reny [23] showed that cathode wear increases with increased $AlF_3$ content. Ødegård et al. [24] also observed in their laboratory tests that the maximum aluminium carbide dissolution occurs at a cryolite ratio of 1.8. This supports the importance of bath acidity for the cathode wear in the case the carbide solubility is a limiting factor. Without continuous supply of fresh bath to maintain the supply of aluminium ions to the cathode surface, the cathode wear process is suggested to slow down or even stop. From the ternary phase diagram $Na_3AlF_6$ -$AlF_3$ -$CaF_2$ [22] it can also be seen that the melting point of the bath increases as it becomes more basic. This change in composition will result in solidification of the electrolyte at the cathode surface and thereby slow down or even stop the cathode wear process. The slow down or stopping of the wear process due to the frozen bath can be related to the relatively low electrical conductivity of the solid electrolyte compared to the molten bath. The cathode wear process being mostly electrochemical in nature [1, 5, 25] need a current to continue, hence a drastic reduction or termination of current density can slow down or stop the wear process. Finally, dissolution of aluminium carbide will also terminate as the bath solidify.

Based on the findings from the autopsy and laboratory analysis, we propose an initiation and termination process in the cathode wear process. The proposed mechanism is as follows:

1. The formation of $Al_4C_3$ is favoured by available $AlF_3$ in the molten bath present at the cathode surface (Reaction 1).
2. The local consumption of $AlF_3$ due to formation of $Al_4C_3$ results in more basic bath, which also reduce the transport of $Al_4C_3$ away from the surface due to the lower solubility of $Al_4C_3$ in basic bath.
3. The reduced content of $AlF_3$ results in an increased liquidus temperature, which will lead to partly or completely solidification of the molten bath close to the cathode surface.
4. Solid bath on the carbon cathode surface will terminate or drastically slow down the wear process due to reduced current density and carbide dissolution. Supply of fresh molten bath with a higher $AlF_3$ content will restart the wear process through re-melting of frozen bath. Increased cathode surface temperature can also re-melt the frozen bath and restart the wear process.

The pitting on all the spent potlinings, especially at locations with highest wear, point to the importance of pitting for the underlying mechanism for carbon cathode wear. Moreover, pitting was observed on all the different grades of carbon blocks (graphitic, graphitized, high density and impregnated) as well as on the more amorphic ramming joints. Current density as well as transport of carbide may, however, affect formation of pitting on carbon cathodes, as they seem to be more pronounced at locations with highest current density such as the side ends. The high current densities at the side ends may induce high magneto-hydrodynamic movements in the metal and bath resulting in faster bath replacement rates and thus higher degree of wear. Pitting on carbon cathodes have been previously explained by Rafiei et al. [1] to occur by a particulate detachment mechanism resulting from weakening of the carbon internal structure due to internal carbide formation in the pores. Evidence for particulate detachment was however not observed in the present autopsies, suggesting that cathode wear and the characteristic pitting occur by a chemical or electrochemical process.

FEM simulations

In order to test the hypothesis presented above, a FEM simulation of the current distribution close to a cathode surface with partly solidified electrolyte was conducted as shown in Figure 7. The results demonstrate that the current density along the cathode block is close to zero at locations with the frozen bath. This implies that the cathode wear process, being electrochemical in nature, will to a large degree be terminated at locations with

precipitation of frozen bath consisting mainly of cryolite. A uniform thickness of the bath was here assumed. The homogeneity of the bath layer is a key issue and should be further investigated both in autopsies and FEM simulations.

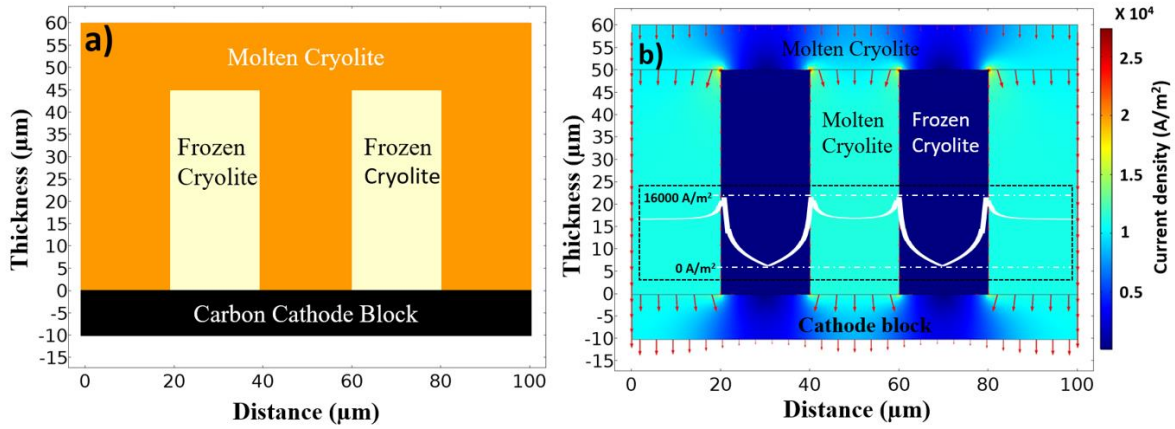


**Figure 7** FEM-COMSOL simulation image, **a** geometry of the thin bath used in the simulation, **b** simulation results, red arrows show the current density distribution, colours represent magnitude of the current density (blue is low and red is high), insert is the current density distribution along the carbon cathode block

## Conclusions

Autopsies of several spent pot linings were conducted in order to investigate carbon cathode wear. Pitting on all carbon cathode types were observed, which demonstrate the importance of pitting in the cathode wear mechanism. The topography of the cathode surface in the area with sever pitting strongly suggest that cathode wear is electrochemical/chemical in nature and not physical or mechanical. A mechanism involving an initiation and termination step in the cathode wear process were proposed involving solidification of the electrolyte on the carbon cathode caused by the formation of aluminium carbide through the depletion and enrichment of $AlF_3$ in the bath

## Acknowledgement

Financial support from the Norwegian Research Council and the partners Hydro, Alcoa, Elkem Carbon and Skamol through the project "CaRMa - Reactivity of Carbon and Refractory Materials used in Metal Production Technology" is acknowledged.

## References

[1] P. Rafiei, F. Hiltmann, M. Hyland, B. James, B. Welch, *Light Metals* 2001, 747 (2001)
[2] F. Gao, N. Feng, J. Yang, Q. Niu, H. He, L. Han, *Light Metals* 2012, 1355 (2012)
[3] M. Sørlie, H.A. Øye, *Cathodes in aluminium electrolysis*, 3rd ed.(Aluminium-Verlag, Düsseldorf, 2010).
[4] A.T. Tabereaux, J.H. Brown, I.J. Eldridge, T.R. Alcorn, *Light Metals* 1999, 187 (1999)
[5] P. Reny, S. Wilkening, *Light Metals* 2000, 399 (2000)
[6] S. Senanu, T. Grande, A.P. Ratvik, *ICSOBA* 41, 787 (2016)
[7] S. Senanu, C. Schøning, S. Rørvik, Z.H. Wang, A.P. Ratvik, T. Grande, *Light Metals* 2017, 561 (2017)
[8] S. Wilkening, P. Reny, B. Murphy, *Light Metals* 2005, 367 (2005)
[9] J.M. Dreyfus, L. Joncourt, *Light Metals* 1999, 199 (1999)
[10] K. Tschöpe, A. Støre, E. Skybakmoen, A. Solheim, T. Grande, A.P. Ratvik, *Light Metals* 2013, 1251 (2013)
[11] P. Patel, M. Hyland, F. Hiltmann, *Light Metals 2005*, 757 (2005)
[12] L.P. Lossius, H.A. Øye, *Met Trans B* 31 (6), 1213 (2000)
[13] E.F. Siew, T. Ireland-Hay, G.T. Stephens, J.J.J. Chen, M.P. Taylor, *Light Metals 2005*, 763 (2005)
[14] S. Senanu, T. Grande, A.P. Ratvik, *ICSOBA* 43, 643 (2018)
[15] M. Sørlie, J. Hvistendahl, H.A. Oye, *Light Metals* 1993, 299 (1993)
[16] M. McClung, R. Zerkle, *Light Metals* 2004, 213 (2004)

[17] R. Jeltsch, *Light Metals* 2009, 1079 (2009)
[18] K. Tschöpe, C. Schøning, J. Rutlin, T. Grande, *Met Trans B* 43 (2), 290 (2012)
[19] K. Tschöpe, C. Schøning, T. Grande, *Light Metals 2009*, 1085 (2009)
[20] E. Skybakmoen, S. Rørvik, A. Solheim, K.R. Holm, P. Tiefenbach, Ø. Østrem, *Light Metals* 2011, 1061 (2011)
[21] J. Thonstad, P. Fellner, G.M. Haarberg, J. Hives, H. Kvande, A. Sterten, *Aluminium Electrolysis: Fundamentals of the Hall-Héroult Process*, 3rd ed.(Aluminium-Verlag Marketing and Kommunikation GmbH, Düsseldorf, 2001).
[22] D.F. Craig, J.J. Brown, *J Am Ceram Soc* 63 (5-6), 254 (1980)
[23] S. Wilkening, P. Reny, *Light Metals* 2004, 597 (2004)
[24] R. Ødegard, A. Sterten, J. Thonstad, *Met Trans B* 19 (3), 449 (1988)
[25] K. Tschöpe, A. Støre, A. Solheim, E. Skybakmoen, T. Grande, A.P. Ratvik, *JOM* 65 (11), 1403 (2013)

List of Figure Captions

Figure 1: Cylindrical sample drilled from the spent potlining for laboratory analysis (CT and microscopy), showing pitting at the surface marked by the blue dotted circle

Figure 2: Images of pitting on the surface of the carbon cathodes. **a** 3D scanning image of a section of pot 5 showing pitting at the ends of the cathode blocks**, b** Variation of pitting size along cathode block from side end to centre channel of the cell from pot 3, the typical pitting are highlighted with a red dashed rectangles**, c** Pitting on both cathode block and ramming joint from pot 5

Figure 3: CT scanning images of the XY, YZ and XZ directions with a highlighted section of the XZ directional view image to illustrate wear profile of binder matrix and aggregate. Pitting locations are marked by blue dotted circle on the XY image. A sketch defining the XY, YZ and XZ directions of the cylindrical cathode sample where the XY plane is normal to the Z-axis is included in the figure.

Figure 4: Optical micrograph of the interface between the carbon cathode and bath in a sample from pot 1

Figure 5: EDS element mapping of carbon-bath interface of samples from pot 6. **a** Element map of cathode surface with sludge (pot 6), **b** Element map of cathode surface with no sludge, **c** Chemical composition of cryolite at interface, **d** Chemical composition of alumina at interface **e** Chemical composition of aluminium carbide at interface

Figure 6: X-ray diffraction pattern of bath samples collected from the bath on top of the metal pad and on top of the cathode surface. Black dashed arrows to trace the identified phases. Insert: sketch of an electrolysis cell showing locations of the solid bath samples

Figure 7: FEM-COMSOL simulation image, **a** geometry of the thin bath used in the simulation, **b** simulation results, arrows show the current density distribution, dark and light areas represent low and high current density areas respectively, insert is the current density distribution along the carbon cathode block